

Sem-NaVAE: Semantically-Guided Outdoor Mapless Navigation via Generative Trajectory Priors

Gonzalo Olguin¹, Javier Ruiz-del-Solar¹

Abstract—This work presents a mapless global navigation approach for outdoor applications. It combines the exploratory capacity of conditional variational autoencoders (CVAEs) to generate trajectories and the semantic segmentation capabilities of a lightweight visual language model (VLM) to select the trajectory to execute. Open-vocabulary segmentation is used to score and select the generated trajectories based on natural language, and a state-of-the-art local planner executes velocity commands. One of the key features of the proposed approach is its ability to generate a large variability of trajectories and to select them and navigate in real-time. The approach was validated through real-world outdoor navigation experiments, achieving superior performance compared to state-of-the-art methods. A video showing an experimental run of the system can be found in <https://www.youtube.com/watch?v=i3R5ey5O2yk>.

Index Terms—Learning from Demonstration, Deep Learning Methods, Reactive and Sensor-Based Planning.

I. INTRODUCTION

AUTONOMOUS navigation in mobile robotics remains one of the most enduring challenges in the field. Although traditional “Map-Plan-Control” approaches have proven effective in structured industrial settings, they rely heavily on pre-defined metric maps and kinematic models that fail to adapt to rapid environmental changes or unforeseen obstacles.

To address these limitations, learning-based methods have gained popularity, offering superior performance in dynamic and unstructured environments by directly capturing complex behaviors from data [1]. These approaches leverage deep learning to navigate changing terrains and variable lighting conditions, integrating visual and range sensors to enhance environmental perception [2], [3], [4].

However, the majority of direct supervised learning approaches face a critical limitation: *unimodality*. In real-world navigation, multiple valid trajectories often exist to bypass an obstacle (e.g., passing a tree on the left or right). Traditional discriminative models tend to average these solutions, resulting in collisions or physically infeasible behaviors [5], [6]. Here, generative models represent a paradigm shift. By learning the probability distribution of possible trajectories rather than a single deterministic output, these models capture the stochastic nature of real-world navigation, proposing multiple feasible and diverse motion hypotheses [7], [8].

However, despite their ability to ensure geometric feasibility, generative models often lack deep semantic understanding.

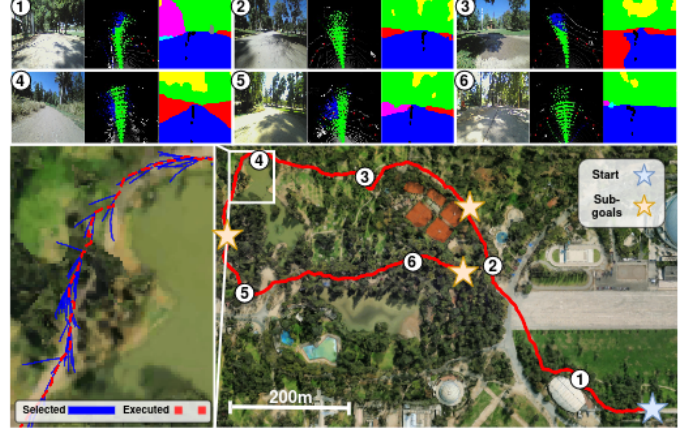


Fig. 1. Examples of autonomous mapless navigation. Six timesteps are shown (1-6) with their corresponding selected and executed paths on a satellite image. Left rows show a First Person View (FPV) of the robot’s onboard camera. Middle rows show an elevation map with the proposed trajectories (blue represents collisions and green dynamically feasible waypoints). Right rows show the selected trajectory projected onto an FPV costmap (in black).

A robot might generate valid paths through both a flowerbed and a paved path; while both are geometrically possible, the choice depends on social norms or contextual constraints that are difficult to encode in a traditional cost function. Recently, Vision-Language Models (VLMs) have emerged as powerful tools for equipping robots with common-sense reasoning [9], [10]. These models bridge the gap between visual perception and logical decision-making, enabling the interpretation of complex scenes and natural language instructions.

In this work, we propose a mapless global navigation framework that combines the exploratory capacity of Conditional Variational Auto-Encoders (CVAEs) in a **trajectory generation module**, with the semantic segmentation capabilities of a lightweight VLM as a **trajectory selection module**. Unlike approaches dependent on maintenance-heavy global metric maps, our system plans long-horizon routes adaptively. We utilize a two-level architecture where our module acts as the high-level planner—using open-vocabulary segmentation to score trajectories and guide navigation based on natural language—while a state-of-the-art local planner executes the velocity commands.

The main contributions of this work are the following:

- **CVAE trajectory generator:** We propose a planning architecture based on CVAE with learned prior for trajectory generation, conditioned on the robot’s sensory observations. It is efficient enough to generate a large number (>200) of movement hypotheses to supply most

This work was partially supported by FONDECYT project 1251823.

¹ Advanced Mining Technology Center (AMTC) and Department of Electrical Engineering, Universidad de Chile, Tupper 2007, Santiago, Chile.

of the available directions of movement.

- **Open vocabulary trajectory selection method:** Takes into account the semantic classes and preferences imposed by the user and the geometric distance to the navigation objective, as well as kinematic constraints by filtering unfeasible trajectories beforehand.
- **Asynchronous update strategy:** Instead of periodically selecting the best trajectory at a fixed frequency, we propose a method to compare running costs of the future waypoints with new ones, switching to a new trajectory only when a cost criterion is met. This method allows the module to correct for occlusions at inference time and better utilize the generated trajectories by not having to change the local planner goals at every time step.

II. RELATED WORK

A. Traversability Estimation and Semantic Perception

To address physical interaction with semantics, early works like [11] correlated visual appearance with robot vibration. This has evolved into deep self-supervised learning, where proprioceptive signals (e.g. torque, velocity) automatically label visual data [12], [13] to later learn cost maps or navigation policies. Models trained from large-scale datasets, such as HDIF [14] and recent work on interaction-aware navigation [15] learn cost functions linking geometry to vehicle dynamics. The visual features of DINO [16] have been used in Velociraptor [17] together with LiDAR to learn risk aware costmaps, and also in WVN [4] to learn a traversability map online using only vision and velocity feedback. Approaches such as ViPlanner [18] fuse semantic labels with depth images to directly predict control actions and prefer safer terrains (e.g., asphalt instead of mud).

Although effective for stability and local safety, these traversability methods often struggle to generalize to semantically distinct environments not seen during training, as they lack a high-level conceptual understanding of the scene.

B. Generative Trajectory Models

A common issue with learned planners in outdoor environments, particularly in complex scenarios, is the *unimodality* of the proposed trajectories. To address this, generative models have emerged as the state of the art. Inspired by the inherent multimodality of human motion, numerous works have employed CVAEs [19], [20] or diffusion models [21], [22] to predict multiple motion hypotheses conditioned on observations such as pedestrian positions or local maps. Translating this paradigm to ego-centric robotic navigation, several studies leverage generative models to synthesize plausible trajectories directly from sensory data. In particular, MTG [23] uses an attention-based CVAE to generate various predictions that maximize spatial coverage. This line of research is further advanced by DTG [24], which replaces CVAE with a diffusion-based predictor to improve the fidelity and stability of generated paths. Similarly, NoMaD [8] employs a unified diffusion policy to model the joint distribution of subgoals and actions in image space, enabling robust exploration and navigation without global maps.

However, even though these methods demonstrate superior capability in generating geometrically feasible and diverse motion plans, they typically lack a semantically grounded selection strategy, often relying on simple heuristics or geometric cost functions to choose the final trajectory.

C. Open vocabulary segmentation and VLMs for robotic navigation

At a higher level, VLMs such as GPT-4 [25] or Gemini [26] have been integrated to interpret natural language commands [9], [27], allowing instruction-following behaviors (e.g., “find a glass in the kitchen”) and even long-range navigation with behavioral cues [10], [28], [29]. However, such systems typically depend on the creation or existence of maps (whether topological or semantic), which presents a significant limitation in terms of scalability and deployment efficiency, as they necessitate prior exploration or the continuous maintenance of updated representations in dynamic environments.

Recent work applied VLMs to low-level control. Methods like PIVOT [30] and ConVOI [31] use VLMs to select trajectories or modulate planner parameters based on context. Other works like BeHaV [32] use lightweight VLMs to perform open vocabulary segmentation with CLIP [33], which enables faster inference for navigation. Closest to our work are TGS [34] and MOSU [35], which employ a “Generate-and-Select” paradigm: a CVAE generates geometrically feasible sub-goals, and a VLM selects the best candidate based on language alignment. MOSU adds a confidence metric and a semantic score based on closed vocabulary segmentation and QGIS routing for long range navigation.

While these works establish a robust baseline, they rely on full scale VLM APIs, which have the problem of needing an internet connection; consequently, they have an inference time on the order of seconds.

III. PROPOSED METHODOLOGY

An overview of the proposed methodology, which includes a CVAE-based trajectory generation module and a VLM-based trajectory selection module, is shown in Fig. 2.

A. Trajectory Generation

1) **Problem formulation:** We consider a robotic agent navigating a dynamic environment equipped with a multimodal perception system. At time step t , the observations vector \mathbf{x} is defined as:

$$\mathbf{x} = \{\mathbf{x}_{\text{lidar}}, \mathbf{x}_{\text{traj}}, \mathbf{x}_{\text{goal}}\}, \quad (1)$$

where:

- $\mathbf{x}_{\text{lidar}} \in \mathbb{R}^{N_l \times N_p \times 4}$ represents the temporal sequence of the last N_l processed point clouds. Each cloud consists of N_p points defined by their spatial coordinates (x, y, z) and intensity: $\{\mathbf{s}_{t-N_l+1}^{\text{lidar}}, \dots, \mathbf{s}_t^{\text{lidar}}\}$.
- $\mathbf{x}_{\text{traj}} \in \mathbb{R}^{N_v \times 4}$ corresponds to the history of the last N_v robot states, comprising position and linear velocity: $\{\mathbf{s}_{t-N_v+1}^{\text{state}}, \dots, \mathbf{s}_t^{\text{state}}\}$.

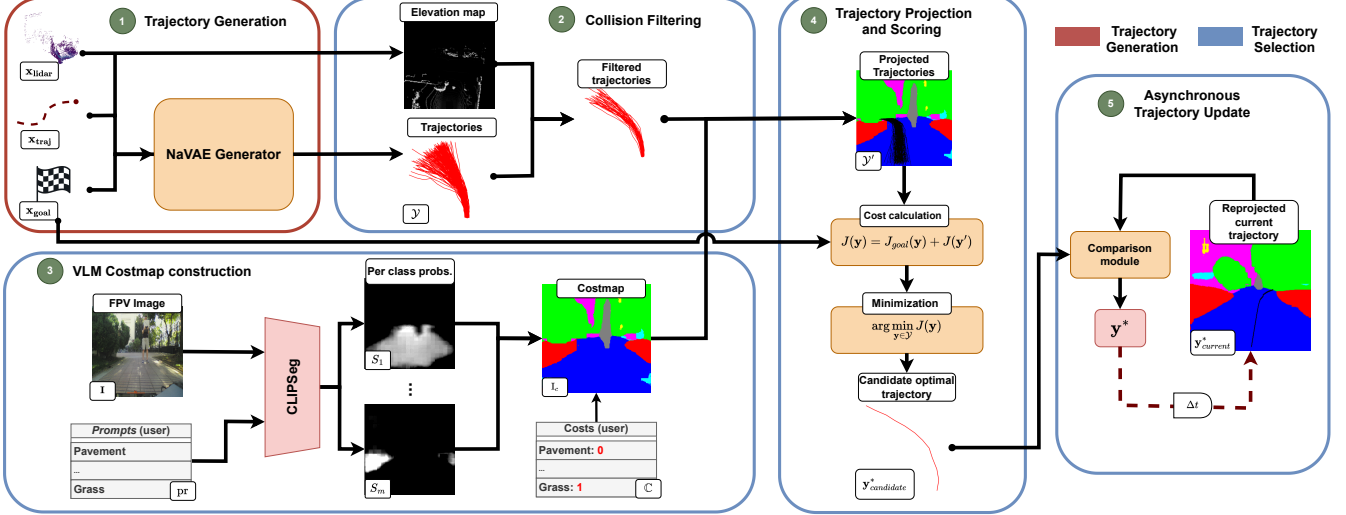


Fig. 2. **Sem-NaVAE overview**: A generator module proposes a number of motion hypotheses based on sensory information. These hypotheses are then filtered by collisions and projected onto and FPV semantic map constructed with a lightweight VLM. Both semantic and goal-distance costs are used to then select the optimal trajectory. Instead of periodically updating to a new trajectory at every inference step, the new best one is compared with the currently executing one, only switching to the new when optimal.

- $\mathbf{x}_{\text{goal}} \in \mathbb{R}^2$ denotes the global navigation goal, expressed in polar coordinates (ρ, θ) relative to the robot's current reference frame.

The objective is to predict the future behavior of the agent over a prediction horizon τ . We define the future trajectory as a sequence of spatial positions $\mathbf{y} = \{\mathbf{p}_{t+1}, \dots, \mathbf{p}_{t+\tau}\}$, where each $\mathbf{p}_k \in \mathbb{R}^2$ corresponds to 2D coordinates in the robot's base frame.

Due to inherent uncertainty in navigation and environmental interaction, the future is stochastic. Multiple physically plausible trajectories exist for a single historical context \mathbf{x} . Therefore, rather than seeking a single point estimate $\hat{\mathbf{y}} = f(\mathbf{x})$, we model future uncertainty via a conditional probability distribution $p(\mathbf{y} | \mathbf{x})$.

Since this underlying distribution can be highly complex and multimodal (encompassing distinct behaviors such as turning left or continuing straight), our goal is to learn a generative model parameterized by ψ that approximates this distribution $p_\psi(\mathbf{y} | \mathbf{x})$.

Operationally, the model is required to generate a diverse set of K hypothetical trajectories $\mathcal{Y} = \{\hat{\mathbf{y}}^{(k)}\}_{k=1}^K$ sampled from the learned distribution:

$$\hat{\mathbf{y}}^{(k)} \sim p_\psi(\mathbf{y} | \mathbf{x}), \quad \text{for } k = 1, \dots, K. \quad (2)$$

Thus, the problem reduces to maximizing the likelihood of the observed real trajectories under the model's predictive distribution, ensuring that the generated set \mathcal{Y} covers the diverse modes of the true future distribution.

To achieve this, we propose an architecture based on CVAEs with a learned prior, following the framework proposed in [20] and [19]. Fig. 3 illustrates the proposed NaVAE (Navigation VAE) architecture, highlighting the main modules: the pre-trained PointNet encoder, the prior encoder, the posterior encoder, and the stochastic decoder.

2) **PointNet Pre-training & Heatmap Generation**: To extract environmental features and constrain the predicted trajectories using teacher forcing, the model integrates a pre-trained PointNet [36] that performs binary segmentation on the voxelized input point cloud $\mathbf{x}_{\text{lidar}}$, classifying points as *traversable* or *non-traversable*.

Ground truth labels are generated by projecting point coordinates onto a global semantic map (available only during training) filtering out points exceeding $1.5 \times$ the robot's height (e.g., tree canopies). The network is trained via a weighted Cross-Entropy loss to address class imbalance.

To condition the trajectory decoder, the sparse point predictions are rasterized in a 2D grid with resolution $\delta = 0.2\text{m}/\text{px}$ and a size of $18\text{m} \times 18\text{m}$. For each cell (u, v) , we compute the mean logit score to ensure invariance to the density of points. The final segmentation heatmap \mathbf{I}_{seg} is obtained by applying a Gaussian smoothing kernel \mathcal{G}_σ ($\sigma = 5$) to propagate semantic information to adjacent empty cells:

$$\mathbf{I}_{\text{seg}} = \mathcal{G}_\sigma * (M^+ - M^- + 1), \quad (3)$$

where M^+ and M^- represent the occupancy grids for traversable and non-traversable logits, respectively.

3) **NaVAE Network Architecture**: The proposed CVAE architecture consists of three core modules: a *Prior Encoder* that captures the current context, a *Posterior Encoder* that is used for training, and a *Decoder* that generates the candidate trajectories.

The prior encoder $p_\theta(z | \mathbf{x})$ processes the context \mathbf{x} to parametrize the latent prior (μ_p, Σ_p) (which then reparametrizes into z_p) and generates a context vector \mathbf{h}_x . It fuses the three input modalities (see Fig. 3):

- **LiDAR**: The voxelized point cloud $\mathbf{x}_{\text{lidar}}$ is processed by the pre-trained PointNet backbone. It outputs a feature vector h_{lidar} via a Fully Connected (FC) layer. Additionally, the segmentation logits are rasterized into a 2D

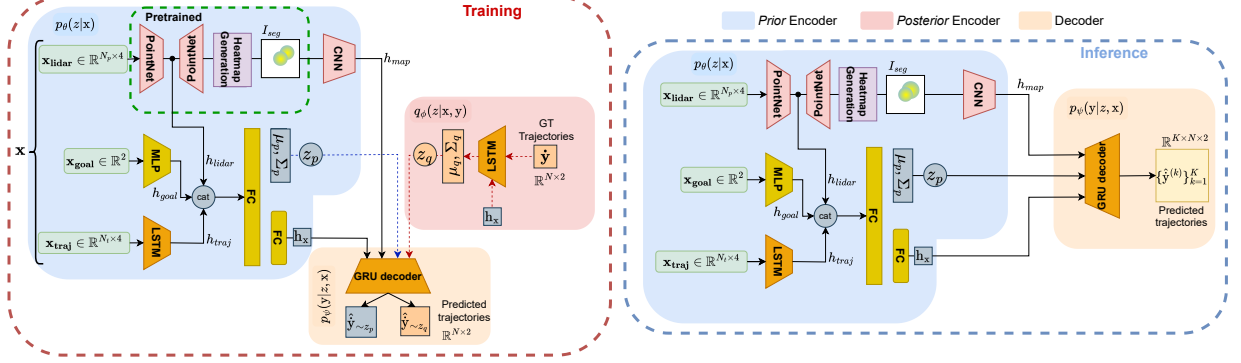


Fig. 3. NaVAE architecture. The model takes as inputs consecutive pointclouds, past trajectory and navigation goal in polar coordinates. A pre-trained PointNet encoder serves as a feature extractor for the conditional value into the CVAE and as heatmap generator for teacher forcing in the GRU decoder. Taking K samples from p_θ yields K predicted trajectories.

Gaussian heatmap \mathbf{I}_{seg} , which is downsampled via CNN to obtain spatial features h_{map} for the decoder.

- **Goal:** The polar goal vector \mathbf{x}_{goal} is processed by a 2-layer MLP to produce h_{goal} .
- **State History:** Past trajectories \mathbf{x}_{traj} (positions and velocities) are encoded by a single-cell LSTM to capture temporal dynamics and produce h_{traj} .

The features are concatenated as $\mathbf{h} = [h_{lidar}; h_{goal}; h_{traj}]$ and passed through LayerNorm and FC layers to produce the final context representation \mathbf{h}_x and the latent parameters (μ_p, Σ_p) .

The posterior encoder $q_\phi(z|x, y)$, available only during training, encodes the ground truth future trajectory y . We utilize a Bidirectional LSTM to process y , allowing the latent state z_q to capture global temporal dependencies (e.g., how the final destination influences initial maneuvering). The output is projected to the latent space parameters (μ_q, Σ_q) .

The decoder $p_\psi(y|z, x)$ operates as an autoregressive generator in velocity space to ensure kinematic smoothness. It is implemented as a GRU, as many other works [20], [23].

At each step t , the GRU receives the latent sample z (both from p_θ and q_ϕ during training, just from p_θ during inference), the context \mathbf{h}_x , and the features of the spatial map h_{map} . It outputs the parameters of a Gaussian distribution over velocities (μ_y, Σ_y) . During inference, we sample velocities \mathbf{v}_t from this distribution, filtering candidates that violate acceleration limits ($> 0.5 \text{ m/s}^2$) or fall into non-traversable regions of \mathbf{I}_{seg} after projection. The final trajectory positions are obtained via numerical integration: $\mathbf{p}_{t+1} = \mathbf{p}_t + \mathbf{v}_t \Delta t$.

4) **Training Objective:** The training objective is based on a CVAE formulation with a learned prior. We minimize a modified Evidence Lower Bound (ELBO) that includes the Kullback-Leibler (KL) divergence between the prior p_θ and posterior q_ϕ , along with the reconstruction likelihoods. Following [20], we enforce reconstruction from the posterior samples z_q and the prior samples z_p to align both distributions with the ground truth:

$$\mathcal{L}_{ELBO} = -\mathbb{E}_{z_p}[\log p_\psi(y|z_p, x)] - \mathbb{E}_{z_q}[\log p_\psi(y|z_q, x)] + \beta D_{KL}(p_\theta||q_\phi). \quad (4)$$

However, standard likelihood maximization tends to average conflicting modes, leading to valid but unrealistic “mean”

trajectories. But we are interested in the general case where the dataset contains M valid ground truth trajectories $\{\mathbf{y}^{(m)}\}_{m=1}^M$ for similar contexts. To capture this diversity, we reformulate the reconstruction loss for the *prior* using a *log-mean-exp* strategy. This is mathematically analogous to Importance Weighted Autoencoders (IWAE) [37], where moving the summation inside the logarithm provides a tighter variational lower bound. Operationally, this acts as a *soft Winner-Takes-All* mechanism: the gradient is dominated by the hypothesis $\mathbf{y}^{(m)}$ that best matches the ground truth. This allows the model to specialize in specific modes without being penalized for not predicting mutually exclusive alternatives.

Crucially, this formulation applies only to the prior (which must cover all modes). The posterior q_ϕ , which is conditioned on a specific ground truth during training, uses standard likelihood. The final reconstruction loss is:

$$\mathcal{L}_{recon} = -\log \left(\frac{1}{M} \sum_{m=1}^M p_\psi(\mathbf{y}^{(m)}|z_p, x) \right) - \mathbb{E}_{z_q}[\log p_\psi(\mathbf{y}|z_q, x)]. \quad (5)$$

Furthermore, to explicitly discourage non-navigable predictions, we introduce a collision loss \mathcal{L}_{col} similar to the one proposed in [23]. Trajectories are projected onto the local semantic ground truth map \mathbf{M}_{sem} . We apply a Gaussian Kernel $\mathbf{GK}(\cdot)$ over the map to smooth the gradients, penalizing waypoints that fall into non-traversable regions:

$$\mathcal{L}_{col} = \log \left(\sum_{(p_x, p_y) \in \mathbf{y}'} \mathbf{GK}(\mathbf{M}_{sem}(p_x, p_y)) \right). \quad (6)$$

The total objective function is a weighted sum:

$$\mathcal{L}_{Total} = \beta D_{KL}(p_\theta||q_\phi) + \mathcal{L}_{recon} + \lambda \mathcal{L}_{col}, \quad (7)$$

where β and λ are regularization hyperparameters.

B. Trajectory Selection

1) **Collision filtering:** Since the generated trajectories can have kinematic failures, a post-generation filter is required to

ensure feasibility. For this, we use a local elevation map [38] constructed from LiDAR data, covering a forward-facing area of $18\text{m} \times 18\text{m}$ with resolution $0.1\text{m}/\text{px}$.

A trajectory is classified as a collision if the pitch angle between any two consecutive waypoints exceeds a safety threshold θ_{max} . For a waypoint w_i and its predecessor w_{i-1} , the inclination is calculated as:

$$\theta_i = \arctan \left(\frac{z_i - z_{i-1}}{\sqrt{\Delta x^2 + \Delta y^2}} \right), \quad (8)$$

where $\Delta x, \Delta y$ are the planar displacements, and z_i is determined by the maximum elevation value within the robot's square footprint d_{foot} centered at (x_i, y_i) . Any trajectory containing a segment where $\theta_i > \theta_{max}$ is discarded. This slope-based constraint effectively filters out step obstacles and untraversable gradients while accounting for the robot's physical dimensions.

2) **VLM Costmap Construction:** Following the generation of dynamically feasible trajectories, the subsequent task is to identify the candidate that best aligns with user-imposed constraints. To achieve this, we employ CLIPSeg [39], a zero-shot model capable of generating pixel-wise probability maps indicating the presence of objects or regions based on natural language queries.

Given a First-Person View (FPV) input image \mathbf{I} and a set of open-vocabulary textual constraints $\mathbf{pr} = \{pr_1, pr_2, \dots, pr_m\}$, CLIPSeg yields a corresponding set of probability maps $\mathbf{S} = \{S_1, S_2, \dots, S_m\}$. Here, each map S_i represents the pixel-wise probability of the constraint pr_i being present within \mathbf{I} . These constraints typically correspond to semantic classes relevant to unstructured outdoor environments, such as "grass," "person" and "stairs". Crucially, these classes are modular and can be dynamically swapped depending on the specific navigation task.

To synthesize a unified semantic cost map \mathbf{I}_c , we assign a scalar cost coefficient to each textual class: $\mathbb{C} = \{c_1, c_2, \dots, c_m\}$. The final cost map is constructed by determining the dominant class at each pixel and assigning the corresponding cost:

$$\mathbf{I}_c(u, v) = \mathbb{C} \left[\arg \max_i (S_i(u, v)) \right], \quad (9)$$

where (u, v) denotes the pixel coordinates and $i \in \{1, \dots, m\}$. The resulting matrix \mathbf{I}_c provides a dense semantic representation of the environment's traversability costs aligned with the user's intent.

3) **Trajectory Projection and Scoring:** The generated trajectories \mathcal{Y} , initially defined in the robot's local frame, must be evaluated against the semantic cost map \mathbf{I}_c . First, a trajectory \mathbf{y} is transformed into the camera frame using the extrinsics $\mathbf{T}_{\mathbf{r}-\mathbf{c}}$ and then projected onto the image plane using the camera intrinsics K :

$$\mathbf{y}' = K[I_3|0]\mathbf{T}_{\mathbf{r}-\mathbf{c}}\mathbf{y}. \quad (10)$$

Here, \mathbf{y}' contains the pixel coordinates (p_x, p_y) corresponding to the trajectory waypoints.

We define the semantic cost $J(\mathbf{y}')$ as the discounted sum of costs, sampled from \mathbf{I}_c . A critical challenge in this 3D-to-2D projection is the loss of depth information; a valid path behind an obstacle might project onto the obstacle's pixels (occlusion). To handle this, we employ a masking mechanism:

$$J(\mathbf{y}') = \sum_{j=1}^N \gamma^j \left[\mathbf{I}_c(p_x^j, p_y^j) \cdot \mathbb{1}_{u_j=0} + C_u \cdot \mathbb{1}_{u_j=1} \right], \quad (11)$$

where $\gamma \in [0, 1]$ is a discount factor for future waypoints, and C_u is a fixed penalty. The binary mask u_j indicates an occlusion; it is set to 1 if the semantic cost at the pixel exceeds a threshold T_{occ} (distinguishing between "soft" traversable terrain and strict obstacles, see Section IV-B), and 0 otherwise.

Finally, to ensure progress toward the target, we incorporate a geometric goal term J_{goal} :

$$J_{goal}(\mathbf{y}) = \alpha_1 \log(1 + d(\mathbf{y}, \text{goal})) + \alpha_2 \frac{|\theta_{end}|}{\pi}, \quad (12)$$

where $d(\cdot)$ is the Euclidean distance to the goal and θ_{end} represents the heading alignment error of the last waypoint. The optimal trajectory \mathbf{y}^* is selected by minimizing the joint cost:

$$\mathbf{y}^* = \arg \min_{\mathbf{y} \in \mathcal{Y}} (J(\mathbf{y}') + J_{goal}(\mathbf{y})). \quad (13)$$

4) **Asynchronous Trajectory Update:** Standard planners often employ a receding horizon strategy, executing only the immediate next step. However, given the semantic uncertainty (e.g., occlusions), blindly discarding the long-term plan is suboptimal. We propose an asynchronous update scheme that balances stability with reactivity.

The system operates on two decoupled frequencies: geometric generation (f_{gen}) and semantic perception (f_{clip}). While the robot executes a selected trajectory (\mathbf{y}_{curr}), its cost is not static; it is re-calculated at (f_{clip}) based on the latest CLIPSeg segmentation. Specifically, the costs of already traversed waypoints are frozen, while future waypoints are re-projected onto the new cost map. This allows the system to refine its estimate as the robot approaches a target, resolving initial occlusions or correcting misclassifications (e.g., distinguishing a shadow from an obstacle) without requiring geometric regeneration.

To determine when to switch trajectories, we compare the re-evaluated cost of \mathbf{y}_{curr} against the best candidate from a newly generated set \mathcal{Y} . To prevent oscillations, a switch is triggered only if the new candidate improves the cost by a hysteresis factor $\epsilon > 0$:

$$J(\mathbf{y}_{new}) < J(\mathbf{y}_{curr}) - \epsilon. \quad (14)$$

This hybrid design ensures that navigation decisions are always based on the most recent visual evidence, while minimizing computational overhead.

C. Recovery Behavior

As a final safeguard, a recovery behavior is implemented to trigger if the robot gets stuck and cannot produce any

valid trajectories. The recovery searches for the nearest angular direction to the goal that is free of collisions, so that the orientation of the robot when a valid path is found is also the closest to the objective.

IV. RESULTS

A. Implementation and Experimental Setup

To train the generative model, we collected a real-world dataset using a Husarion Panther UGV equipped with a 64-channel Ouster LiDAR, a generic RGB camera, IMU, and GPS-RTK. Data collection was carried out on the engineering campus of the University of Chile, an unstructured urban environment characterized by pedestrian paths, vegetation, and significant elevation changes.

To enable multimodal learning, we implemented a post-processing pipeline using the recorded ROS bags. For each data sample, we utilized the ROS NavFN planner to generate synthetic valid paths from the robot's current pose to all reachable frontiers within a radius $R_{max} = 15m$ on a static semantic map, constructed with AMCL and satellite image overlays. Candidate paths were filtered to ensure diversity, retaining only those with a Final Displacement Error (FDE) $> 0.5m$ relative to others.

The final dataset comprises 1,706 samples derived from 15 full navigation runs sliced at 0.5s intervals. Each sample contains a slice of the global map, the ground truth trajectories, voxelized LiDAR and corresponding odometry data aligned with the map slice.

It is important to note that the semantic maps are utilized exclusively for training supervision and offline evaluation; they are **not available** to the robot during online inference.

We choose $N_l = 3$, $N_p = 2,560$ and use the last 5 seconds of trajectory data at 0.5 second intervals, with velocity normalized by the maximum of 2m/s. We predict $k = 200$ trajectories in each step with $N_w = 12$ waypoints each at a temporal distance of 1 second. The feature size is set to 256 and the latent space dimension N_z to 512.

We train 1,000 epochs on an NVIDIA RTX4070 device for about 7 hours. We use AdamW optimizer with a learning rate of 0.001 and an exponential scheduler every 10 epochs. We use β as a KL annealing factor to regularize the latent space after a good reconstruction performance is achieved. The collision loss weight α is set to 10. All tests are conducted using a state-of-the-art local planner based on Reinforcement Learning (RL) [40].

B. Quantitative results

To assess the efficiency and effectiveness of the navigation system, we employ the following metrics:

- **Success Rate (SR):** The percentage of episodes in which the robot reaches the goal within a 5 meter threshold.
- **Success weighted by Path Length (SPL):** A standard measure of path efficiency conditioned on success. It is defined as:

$$SPL = \frac{1}{N} \sum_{i=1}^N S_i \frac{d_i}{\max(p_i, d_i)}, \quad (15)$$

where S_i is the binary success indicator, p_i is the actual path length, and d_i is the reference path length. *Note: Due to the dynamic nature of the testing environment (changing obstacles), we use the distance of a human-demonstrated (teleoperated) trajectory as d_i rather than a geometric shortest path (e.g., A*).*

- **Executed Path Traversability (EPT):** The percentage of the robot's *executed* trajectory that remains within preferred "soft" traversable zones. We distinguish between *strict* obstacles (walls, trees) that cause collision/failure and *soft* obstacles (grass, dirt) that are traversable but may be semantically undesirable
- **Non-Traversable Rate (NTR):** The percentage of *generated* waypoints that fall into non-traversable regions (both soft and strict), as defined in [23]. This evaluates the model ability to learn semantic constraints during inference, independent of the final selected path.
- **Navigation Time Ratio (T_{ratio}):** The ratio between the autonomous navigation time and the teleoperated time (T_{nav}/T_{teleop}).
- **Recovery Behaviors (#RB):** The average frequency of local planner recovery trigger events per run.

For trajectory generation, we use **MTG** as a baseline, together with our VLM-based trajectory selection module. We also use a mixed method, which we call **MTG'**, in which MTG is retrained with our PointNet module. This is because, as will become clear when we present the results, MTG produces paths with low variability. In addition, our ablation study considers the use of a different VLM (GPT) for trajectory selection.

The experiments were conducted in an unseen sector of the engineering campus of the University of Chile during training, in 5 different configurations ranging from 120 to 240 meters in length. Each trial was repeated 6 times. The baseline selection parameters $\gamma, \alpha_1, \alpha_2$ are set to 0.8, 2, 0.2, respectively, and the frequencies f_{gen}, f_{clip} are set to 0.5 and 2.5 Hz, respectively. The classes and costs used are: 'pavement' (0), 'tree' (3), 'grass' (2), 'wall' (3), 'stairs' (3), 'person' (3), 'hole' (3), 'sky' (4), and C_u, T_{occ} are both set to 2, as this is the maximum soft-traversable class value.

As shown in Table I, Sem-NaVAE outperforms baselines in SR, EPT, and T_{ratio} , achieving improvements of 27%, 4.3%, and 44%, respectively. Although the NTR metric remains comparable to the MTG' baseline —due to the model's generative diversity producing some infeasible candidates—the selection module effectively filters these out and selects the navigable ones, resulting in superior EPT scores. It can be observed from Fig. 4 that, apart from the larger number of generated trajectories, these present more complex curves that allow the global path followed to be smoother and make less calls to the recovery behavior.

C. Qualitative results

We conducted two additional experiments. First, we vary the cost of specific classes and add a new class to demonstrate the effectiveness of open-vocabulary segmentation with CLIPSeg. The bottom of Fig. 5 shows how varying the cost of the

TABLE I
COMPARISON OF MTG [23], MTG WITH OUR MODIFICATIONS AND OUR MODEL, SEM-NAVAE.

Model	SR \uparrow	SPL \uparrow	EPT% \uparrow	NTR% \downarrow	T _{ratio} \downarrow	#RB \downarrow
Sem-NAVAE	0.90	0.76	95.0	23.4	1.33	2
MTG'	0.63	0.63	90.7	22.1	2.41	3
MTG	0.17	0.16	77.5	32.7	2.62	4

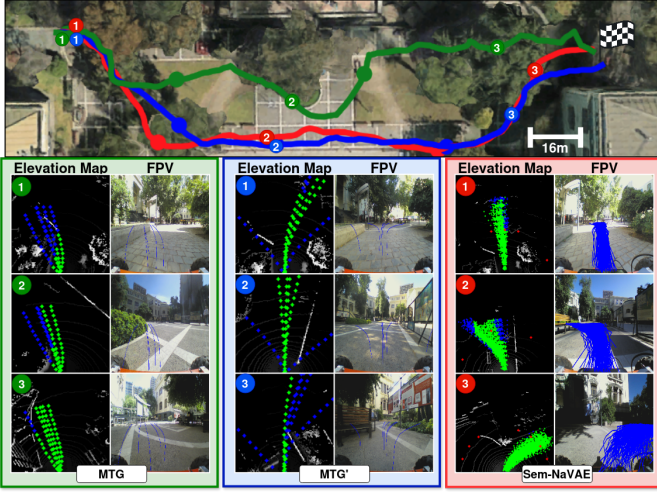


Fig. 4. Comparison of generation baselines MTG [23], its PointNet modification MTG', and our system Sem-NAVAE. Left rows show an elevation map with the proposed trajectories (blue represents collisions and green free-space) and right rows show the generated trajectories projected onto an FPV image.

grass class leads to different behaviors, such as taking shorter paths when the cost is low. The top of Fig. 5 shows that this behavior is also observed for a new class, such as *sand*, which is considered as normal pavement when not present. When present, it can be ignored if the cost is increased.

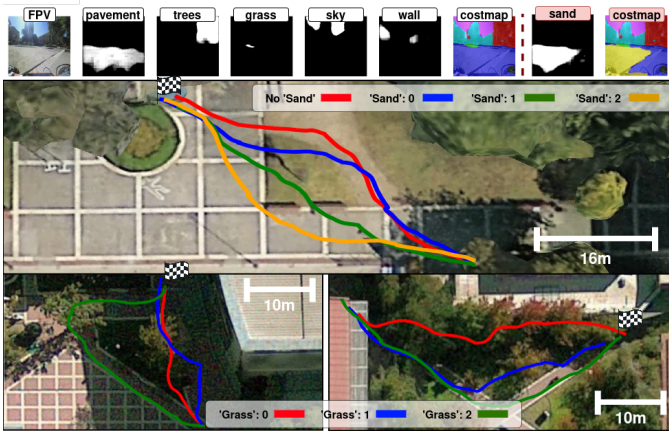


Fig. 5. Comparison of followed trajectories when varying selection classes and costs.

Second, we conducted a long-range navigation test in an urban park using GPS odometry. Fig. 1 shows the path followed and a close up to the selected trajectories. It can be observed that the robot can navigate successfully through a novel environment in a long range setting ($>1\text{km}$) with minimal intervention and without the need for maps, just

GPS odometry. It is noticeable that the selected trajectories are not within a constant interval and that many of them are not entirely feasible; however, the selector module is capable of switching at the right moment to prevent collisions or traversing unwanted terrain.

D. Ablation study

To further test our system, we conducted ablation studies on the trajectory generation and selection modules, as well as on the local planner used and the update policy: (i) Two variations of NaVAE are compared, one with the standard MUSE-VAE loss [20] (**Sem-NAVAE-BaseL**) and the other without collision loss (**Sem-NAVAE-NoCol**). (ii) For trajectory selection, we tested a full-scale VLM API (**NaVAE-GPT**) used in the same fashion as [34], i.e., limiting the output number to the 6 (non-colliding) most diverse trajectories in terms of FDE. (iii) As local planner, we tested using the DWA local planner (**Sem-NAVAE-DWA**) instead of the RL based one. (iv) We tested the use of a synchronous update coupled with the generation frequency (**NaVAE-FixF**), which means the best trajectory is selected at every inference step.

TABLE II
ABLATION STUDY OF SEM-NAVAE.

Model	SR \uparrow	SPL \uparrow	EPT% \uparrow	NTR% \downarrow	T _{ratio} \downarrow	#RB \downarrow
Sem-NAVAE	6/6	0.82	94.5	23.8	1.34	1
Sem-NAVAE-BaseL	2/6	0.13	84.5	54.0	1.56	5
Sem-NAVAE-NoCol	2/6	0.24	82.2	43.5	1.41	4
Sem-NAVAE-DWA	6/6	0.80	95.2	23.2	1.40	2
NaVAE-FixF	4/6	0.69	90.7	23.5	1.37	3
NaVAE-GPT	2/6	0.17	87.8	24.0	4.25	5

Two navigation experiments involving two different routes were conducted, each repeated three times. Table II shows the most relevant results. Firstly, it can be seen that using a different loss function considerably reduces performance, primarily due to reduced prediction diversity and increased collisions. Secondly, the GPT method does not perform well in selecting the trajectory, primarily because it is unable to update the trajectory constantly based on the most recent information. Updates are only made when a trajectory is completed, so the entire navigation task is slower and not in real time. Thirdly, using a fixed update frequency also produces worse results, as this approach may revert to a trajectory that is no better than the previous one. Given the lack of global information, this can be problematic in local minima where the robot can become trapped. Fourth, the performances obtained using the DWA and RL planners are similar. This is as expected, since the system is agnostic to the local planner, provided that it has good obstacle avoidance capabilities to account for unseen obstacles in the generator and selector modules.

V. CONCLUSION

This work addressed the challenge of autonomous navigation in outdoor environments without pre-existing maps. By decoupling motion generation from semantic decision-making, we validated a “Generate-and-Select” architecture that combines the probabilistic exploration of CVAEs with the open-vocabulary reasoning of VLMs.

Our results show that this hybrid approach successfully overcomes the limitations of unimodality in regression-based methods and the semantic inflexibility of purely geometric planners. The proposed CVAE successfully modeled the stochastic nature of navigation by generating diverse, physically feasible hypotheses. The integration of CLIPSeg enabled the robot to adapt its behavior to variable user constraints in real time. Additionally, the asynchronous update mechanism was resilient to temporal occlusions, ensuring safe operation in dynamic real-world scenarios.

REFERENCES

- [1] S. Grigorescu, B. Trasnea, T. Cocias, et al., “A Survey of Deep Learning Techniques for Autonomous Driving,” *Journal of Field Robotics*, vol. 37, no. 3, pp. 362–386, 2020.
- [2] Y.-H. Kim, J.-I. Jang, and S. Yun, “End-to-End Deep Learning for Autonomous Navigation of Mobile Robot,” in *IEEE International Conference on Consumer Electronics (ICCE)*, 2018, pp. 1–6.
- [3] X. Ruan, D. Ren, X. Zhu, et al., “Mobile Robot Navigation Based on Deep Reinforcement Learning,” in *Chinese Control And Decision Conference (CCDC)*, 2019, pp. 6174–6178.
- [4] J. Frey, M. Mattamala, N. Chebrolu, et al., “Fast Traversability Estimation for Wild Visual Navigation,” in *Proceedings of Robotics: Science and Systems (RSS)*, 2023.
- [5] F. Codevilla, M. Müller, A. López, V. Koltun, and A. Dosovitskiy, “End-to-end driving via conditional imitation learning,” in *2018 IEEE International Conference on Robotics and Automation (ICRA)*, 2018, pp. 4693–4700.
- [6] P. Florence, C. Lynch, A. Zeng, O. A. Ramirez, et al., “Implicit behavioral cloning,” in *Conference on Robot Learning*, PMLR, 2022, pp. 158–168.
- [7] A. Gupta, J. Johnson, L. Fei-Fei, et al., “Social GAN: Socially Acceptable Trajectories with Generative Adversarial Networks,” in *IEEE Conference on Computer Vision and Pattern Recognition (CVPR)*, 2018, pp. 2635–2644.
- [8] A. Sridhar, D. Shah, C. Glossop, et al., “NoMaD: Goal Masked Diffusion Policies for Navigation and Exploration,” in *IEEE International Conference on Robotics and Automation (ICRA)*, 2024, pp. 12224–12230.
- [9] D. Song, J. Liang, A. Payandeh, et al., “VLM-Social-Nav: Socially Aware Robot Navigation Through Scoring Using Vision-Language Models,” *IEEE Robotics and Automation Letters*, vol. 10, no. 1, pp. 508–515, 2025.
- [10] D. Shah, B. Osinski, B. Ichter, and S. Levine, “LM-Nav: Robotic Navigation with Large Pre-Trained Models of Language, Vision, and Action,” in *Proceedings of the 6th Conference on Robot Learning (CoRL)*, PMLR, 2022, pp. 259–269.
- [11] S. Thrun, M. Montemerlo, H. Dahlkamp, D. Stavens, et al., “Stanley: The robot that won the darpa grand challenge,” *Journal of Field Robotics*, vol. 23, no. 9, pp. 661–692, 2006.
- [12] L. Wellhausen, A. Dosovitskiy, R. Ranftl, et al., “Where Should I Walk? Predicting Terrain Properties From Images Via Self-Supervised Learning,” *IEEE Robotics and Automation Letters*, vol. 4, no. 2, pp. 1509–1516, 2019.
- [13] C. Jung and D. H. Shim, “Incorporating Multi-Context Into the Traversability Map for Urban Autonomous Driving Using Deep Inverse Reinforcement Learning,” *IEEE Robotics and Automation Letters*, vol. 6, no. 2, pp. 1662–1669, 2021.
- [14] M. Guaman Castro et al., *How does it feel? self-supervised costmap learning for off-road vehicle traversability*, IEEE, 2023.
- [15] P. Schoch, F. Yang, Y. Ma, et al., “IN-Sight: Interactive Navigation through Sight,” in *IEEE/RSJ International Conference on Intelligent Robots and Systems (IROS)*, 2024, pp. 7794–7800.
- [16] M. Caron, H. Touvron, I. Misra, et al., “Emerging Properties in Self-Supervised Vision Transformers,” in *IEEE/CVF International Conference on Computer Vision (ICCV)*, 2021, pp. 9630–9640.
- [17] S. Triest, M. Sivaprakasam, S. Aich, et al., “Velociraptor: Leveraging Visual Foundation Models for Label-Free, Risk-Aware Off-Road Navigation,” in *Proceedings of the 8th Conference on Robot Learning (CoRL)*, PMLR, 2024.
- [18] P. Roth, J. Nubert, F. Yang, et al., “ViPlanner: Visual Semantic Imperative Learning for Local Navigation,” in *IEEE International Conference on Robotics and Automation (ICRA)*, 2024, pp. 5243–5249.
- [19] T. Salzmann, B. Ivanovic, P. Chakravarty, and M. Pavone, “Trajectory++: Multi-Agent Generative Trajectory Forecasting With Heterogeneous Data for Control,” in *European Conference on Computer Vision (ECCV)*, 2020, pp. 683–700.
- [20] M. Lee, S. S. Sohn, S. Moon, et al., “Multi-Scale VAE for Environment-Aware Long Term Trajectory Prediction,” in *IEEE/CVF Conference on Computer Vision and Pattern Recognition (CVPR)*, 2022, pp. 8110–8119.
- [21] C. M. Jiang, A. Cornman, C. E. Park, et al., “MotionDiffuser: Controllable Multi-Agent Motion Prediction Using Diffusion,” in *IEEE/CVF Conference on Computer Vision and Pattern Recognition (CVPR)*, 2023, pp. 9644–9653.
- [22] T. Gu, G. Chen, J. Li, et al., “Stochastic Trajectory Prediction via Motion Indeterminacy Diffusion,” in *IEEE/CVF Conference on Computer Vision and Pattern Recognition (CVPR)*, 2022, pp. 17092–17101.
- [23] J. Liang, P. Gao, X. Xiao, et al., “MTG: Mapless Trajectory Generator with Traversability Coverage for Outdoor Navigation,” in *IEEE International Conference on Robotics and Automation (ICRA)*, 2024, pp. 2396–2402.
- [24] J. Liang, A. Payandeh, D. Song, X. Xiao, and D. Manocha, “DtG : Diffusion-based trajectory generation for mapless global navigation,” in *IEEE/RSJ International Conference on Intelligent Robots and Systems (IROS)*, 2024, pp. 5340–5347.
- [25] O. team, *Gpt-4 technical report*, 2024. arXiv: 2303.08774 [cs.CL].
- [26] G. Team, *Gemini: A family of highly capable multimodal models*, 2025. arXiv: 2312.11805 [cs.CL].
- [27] A. Werby, C. Huang, M. Büchner, et al., “Hierarchical Open-Vocabulary 3D Scene Graphs for Language-Grounded Robot Navigation,” in *Proceedings of Robotics: Science and Systems*, Delft, Netherlands, 2024.
- [28] M. Chang, T. Gervet, M. Khanna, et al., “GOAT: Go to Any Thing,” in *Robotics: Science and Systems (RSS)*, 2024.
- [29] M. Elnoor, K. Weerakoon, G. Seneviratne, et al., “VLM-GroNav: Robot Navigation Using Physically Grounded Vision-Language Models in Outdoor Environments,” in *IEEE International Conference on Robotics and Automation (ICRA)*, 2025, pp. 2391–2398.
- [30] S. Nasiriany, F. Xia, W. Yu, et al., *PIVOT: Iterative Visual Prompting Elicits Actionable Knowledge for VLMS*, arXiv preprint arXiv:2402.07872, 2024. arXiv: 2402.07872 [cs.RO].
- [31] A. J. Sathyamoorthy, K. Weerakoon, M. Elnoor, et al., “CoNVOI: Context-Aware Navigation Using Vision Language Models in Outdoor and Indoor Environments,” in *Proceedings of the 8th Conference on Robot Learning (CoRL)*, PMLR, 2024.
- [32] K. Weerakoon et al., “Behav: Behavioral rule guided autonomy using vlms for robot navigation in outdoor scenes,” in *2025 IEEE International Conference on Robotics and Automation (ICRA)*, 2025, pp. 7044–7051.
- [33] A. Radford, J. W. Kim, C. Hallacy, et al., “Learning Transferable Visual Models From Natural Language Supervision,” in *International Conference on Machine Learning (ICML)*, PMLR, 2021, pp. 8748–8763.
- [34] D. Song, J. Liang, X. Xiao, and D. Manocha, “VL-TGS: Trajectory Generation and Selection Using Vision Language Models in Mapless Outdoor Environments,” *IEEE Robotics and Automation Letters*, 2025.
- [35] J. Liang, K. Weerakoon, D. Song, et al., *MOSU: Autonomous Long-Range Robot Navigation with Multi-Modal Scene Understanding*, arXiv preprint arXiv:2507.04686, 2025. arXiv: 2507.04686 [cs.RO].
- [36] C. R. Qi, H. Su, K. Mo, et al., “PointNet: Deep Learning on Point Sets for 3D Classification and Segmentation,” in *IEEE Conference on Computer Vision and Pattern Recognition (CVPR)*, 2017, pp. 77–85.
- [37] Y. Burda, R. B. Grosse, and R. Salakhutdinov, “Importance weighted autoencoders,” in *Conference on Learning Representations (ICLR)*, Y. Bengio and Y. LeCun, Eds., 2016.
- [38] P. Fankhauser, M. Bloesch, C. Gehring, et al., “Robot-Centric Elevation Mapping with Uncertainty Estimates,” in *International Conference on Climbing and Walking Robots (CLAWAR)*, 2014, pp. 433–440.
- [39] T. Lüddecke and A. Ecker, “Image segmentation using text and image prompts,” in *Proceedings of the IEEE/CVF Conference on Computer Vision and Pattern Recognition (CVPR)*, 2022, pp. 7086–7096.
- [40] F. Leiva and J. Ruiz-del-Solar, *Combining RL and IL Using a Dynamic, Performance-Based Modulation over Learning Signals and Its Application to Local Planning*, arXiv preprint arXiv:2405.09760, 2024. arXiv: 2405.09760 [cs.RO].